

Plume divergence in the Hall thruster due to plasma pressure

IEPC-2007-234

*Presented at the 30th International Electric Propulsion Conference, Florence, Italy
September 17-20, 2007*

Avi Cohen-Zur ^{*1, 2}, Amnon Fruchtman ^{†1}, and Alon Gany ^{‡2}

¹*Holon Institute of Technology, Holon, 58102, Israel*

²*Technion-Israel Institute of Technology, Haifa, 32000, Israel*

Abstract: The Plume divergence in the Hall thruster due to the plasma pressure is analyzed by deriving and solving envelope equations. The evolution of the electron temperature and the radial expansion of the plasma beam are calculated self-consistently. The rate of decrease of the electron temperature due to the plasma radial expansion is affected by heat conduction along the plasma propagation. For the annular plasma jet exiting the Hall thruster, approximated as a slab, it is found that if the coefficient of the heat conductivity is large the cooling of the electrons of the expanding plasma beam is small and consequently the plume divergence is larger. For the plasma beam approximated as cylindrical beyond the point at which it crosses the thruster axis, we show that a large heat conduction does not slow the electron cooling. The plume divergence due to the plasma pressure is therefore smaller. The electron temperature is also affected by the intensity of the magnetic field beyond the cathode. A radial magnetic field at the thruster exhaust inhibits a large cross-field heat flux. On one hand, the smaller heat conductivity of the magnetized plasma results in a cooling of the electrons as they cross the magnetic field. On the other hand however, the reduced mobility of the magnetized electrons results in an ambipolar electric field that tends to heat the electrons. We show that there is an optimal intensity of the magnetic field, at which the temperature of the electrons that cross the magnetic field is minimal and at which, therefore, the plume divergence is minimal.

*Graduate student, Faculty of Aerospace Engineering, aerbnac@aerodyne.technion.ac.il.

†Professor, Sciences Department, fnfrucht@hit.ac.il.

‡Professor, Faculty of Aerospace Engineering, gany@techunix.technion.ac.il.

Nomenclature

a	= plume width
B	= magnetic field intensity
c	= plasma sonic velocity
d	= geometry exponent
k	= reciprocal of a
m_i, m_e	= ion, electron mass
n	= quasineutral plasma density
q	= conducted heat
r	= radial coordinate in cylindrical geometry
S	= cross section area of the beam
s	= entropy
T_e	= electron temperature
u	= dimensionless radial velocity in the envelope formalism
v	= dimensionless axial velocity in the envelope formalism
v_r, v_z	= radial, axial velocity component
z	= axial coordinate
$\alpha, \alpha_1, \alpha_2$	= averaging parameters in the envelope equations
α_B	= Bohm diffusion coefficient
Δ	= dimensionless conducted heat
Γ_0	= particle flux
Γ_ε	= energy flux
κ	= coefficient of heat conductivity
ν	= collision frequency
ξ	= dimensionless axial coordinate
ω_c	= electron cyclotron frequency

I. Introduction

A crucial issue in the Hall thruster performance is achieving a better plume collimation. Decreasing the plume divergence should reduce the erosion of surfaces, especially the solar panels, by impacting ions. Also, a less divergent plume should result in a smaller interference with the RF transmission that is used for communication. Two major sources for the plume divergence are the curvature of the magnetic field lines and the radial force exerted on the plasma by the electron pressure. A considerable theoretical and experimental effort has been made over the past few years in order to understand the evolution of the plume.^{1–22} Encouraging indications for a reduction of plume divergence have been found when the magnetic field configuration²¹ or the electrodes¹¹ were manipulated. We have recently analyzed the role of the magnetic field curvature in increasing the plume divergence and made suggestions as to what magnetic field profile can minimize that divergence.²⁰ In the present paper we analyze the effect of the plasma (electron) pressure on the plume divergence, which, outside the acceleration region, seems to be the main reason for the plume divergence.

The Plume divergence in the Hall thruster due to the plasma pressure is analyzed by deriving and solving a set of envelope equations. The evolution of the electron temperature and the radial expansion of the plasma beam are calculated self-consistently. Although our envelope equations cannot provide as detailed a picture of the plume as some of the numerical simulations do, they have the advantage, due to their simplicity, of allowing a calculation of the plasma flow up to a large distance. This is done by requiring the plasma flow to satisfy appropriate boundary conditions at infinity. In addition, we derive analytical expressions for the flow at asymptotic limits that provide us with a useful insight into the physical processes that govern the plume divergence.

Since the source of the plume divergence is the plasma pressure the extent of the divergence depends on the evolution of the electron temperature. If both magnetic field and heat conductivity are zero the electron temperature decreases adiabatically to zero as the plasma expands and the asymptotic value of the plasma perpendicular velocity can be determined analytically. The rate of decrease of the electron temperature due to the plasma radial expansion is affected by heat conduction along the plasma propagation. For the annular plasma jet exiting the Hall thruster, approximated as a slab, it is found that if the coefficient of the heat conductivity is large the cooling of the electrons of the expanding plasma beam is small and consequently the plume divergence is larger. For the plasma beam, approximated as cylindrical beyond the point at which it crosses the thruster axis, we show that a large heat conduction does not slow the electron cooling. The plume divergence due to the plasma pressure is therefore smaller.

The electron temperature is also affected by the magnitude of the magnetic field beyond the cathode. A radial magnetic field at the plasma exhaust inhibits a large cross-field heat flux. On one hand, the smaller heat conductivity of the magnetized plasma results in a cooling of the electrons as they cross the magnetic field. On the other hand however, the reduced mobility of the magnetized electrons results in an ambipolar electric field that tends to heat the electrons. We show that there is an optimal intensity of the magnetic field, at which the temperature of the electrons that cross the magnetic field is minimal and at which, therefore, the plume divergence is minimal.

In Section II we present the two-dimensional equations and in Section III we derive the envelope equations. These equations allow us to address the inherently two-dimensional problem by simply solving a set of ordinary differential equations. In Section IV we reanalyze the isothermal case^{16,17} that provides us with an upper bound on the plume divergence for a given initial electron temperature. In Section V we numerically solve the evolution of a slab plasma beam with a finite heat conductivity. The above-mentioned two opposite effects of the magnetic field are shown and discussed, following an earlier version of this analysis.¹⁸

In Sections VI and VII the very different effects of heat conduction on the plume divergence for the two geometries are described. In Section VI the effect of the heat conductivity on the divergence of a slab beam is analyzed. We present in more detail a previous analysis¹⁹ that includes analytical expressions for the plume divergence for an asymptotically large coefficient of the heat conductivity. It is shown that the large amount of conducted heat by a slab beam is converted downstream into electron thermal energy and consequently into a large radial velocity and a large divergence of the plasma beam.

Beyond the point at which it crosses the thruster axis we approximate the plasma beam as cylindrical. We show in Section VII that the heat conducted by a cylindrical beam is decoupled from the electron thermal energy convected by the plasma beam. The plume divergence in the cylindrical case is therefore smaller.

II. The two-dimensional equations

We describe here a quasi-neutral azimuthally symmetric plasma beam propagating in the z direction across a magnetic field. We approximate the magnetic field as having a r component only, perpendicular to the direction of the beam, and neglect the axial, z component. The plasma current has an azimuthal component only. We therefore model the plasma beam by writing fluid equations for the identical ion and electron density n and radial and axial velocities, v_r and v_z . Since in the Hall thruster the ion temperature is much smaller than the electron temperature T_e , we take the ion temperature in the model as zero. We also assume that the ions are unmagnetized. The plasma dynamics is therefore governed by the continuity equation

$$\frac{1}{r} \frac{\partial}{\partial r} (r n v_r) + \frac{\partial}{\partial z} (n v_z) = 0, \quad (1)$$

the two components of the momentum equation

$$\begin{aligned} \frac{1}{r} \frac{\partial}{\partial r} (r m_i n v_r^2) + \frac{\partial}{\partial z} (m_i n v_z v_r) &= -\frac{\partial}{\partial r} (n T_e), \\ \frac{1}{r} \frac{\partial}{\partial r} (r m_i n v_r v_z) + \frac{\partial}{\partial z} (m_i n v_z^2) &= -\frac{\partial}{\partial z} (n T_e) - m_e n v_z \frac{\omega_c^2}{\nu}, \end{aligned} \quad (2)$$

and the energy equation

$$\frac{1}{r} \frac{\partial}{\partial r} \left\{ \left[\frac{m_i}{2} (v_r^2 + v_z^2) + \frac{5}{2} T_e \right] r n v_r \right\} + \frac{\partial}{\partial z} \left\{ \left[\frac{m_i}{2} (v_r^2 + v_z^2) + \frac{5}{2} T_e \right] n v_z \right\} = -\frac{1}{r} \frac{\partial (r q_r)}{\partial r} - \frac{\partial q_z}{\partial z}, \quad (3)$$

where m_i and m_e are the ion and electron masses, ν and $\omega_c = eB/m_e$ are the electron collision and cyclotron frequencies, and $q_{z,r}$ is the heat flux in the z, r direction. Also e and B are the elementary charge and the intensity of the radial magnetic field. The second term on the right hand side (RHS) of the second of Eq. (2) expresses the axial magnetic force due to the azimuthal electron current and the radial magnetic field.

For completion we also derive in a standard way the equation for the entropy. Employing Eqs. (1)-(3), we write the heat balance equation for the electrons $n T_e \vec{\nabla} \cdot \vec{v} + \vec{\nabla} \cdot (3/2) n T_e \vec{v} + \vec{\nabla} \cdot \vec{q} = m_e n v_z^2 \omega_c^2 / \nu$, in which the last term on the RHS is the rate of heating. Using the identity $\vec{\nabla} \cdot (n T_e \vec{v}) = n \vec{v} \cdot \vec{\nabla} T_e$ we then derive the equation $T_e \vec{\nabla} \cdot s n \vec{v} + \vec{\nabla} \cdot \vec{q} = m_e n v_z^2 \omega_c^2 / \nu$ for the entropy per particle $s \equiv \ln (T_e^{3/2} / n)$. In cylindrical coordinates this equation becomes

$$T_e \left[\frac{1}{r} \frac{\partial (r s n v_r)}{\partial r} + \frac{\partial (s n v_z)}{\partial z} \right] = -\frac{1}{r} \frac{\partial (r q_r)}{\partial r} - \frac{\partial q_z}{\partial z} + m_e n v_z^2 \frac{\omega_c^2}{\nu}. \quad (4)$$

This equation shows clearly that the entropy flux is constant in the absence of heating and heat conduction.

In the next section we derive a set of envelope equations.

III. The envelope equations

We address two specific cases, both of interest to the Hall thruster. One case is of a thin annular beam that is approximated as a planar slab in which r_0 is the inner radius of the annulus. The second case is of a solid cylindrical beam in which $r_0 = 0$ denotes the axis of symmetry. We derive envelope equations that are suitable for the two cases, either a thin annular beam¹⁸ or a solid cylindrical beam. We integrate the above equations multiplied by $2\pi r$ with respect to r between $r = r_0$ and $r = r_1$, where r_1 denotes the outer edge of the beam. The plasma beam as it exits the thruster channel can be approximated by the slab beam of the first case, while after it expands radially and crosses the thruster cylindrical axis, it can be described by the cylindrical beam of the second case. In both cases, as a result of the radial integration over the entire plume we obtain quasi one-dimensional equations for the radially-average plasma variables at each axial location.

Since there is no net radial flux, all first terms on the left hand side (LHS) of Eqs. (1)-(3) vanish upon the radial integration. So does the first term on the RHS of Eq. (3). The integrated equations are the continuity equation

$$\Gamma(z) \equiv \int_{r_0}^{r_1} 2\pi r n v_z dr = \Gamma_0 = \text{const.}, \quad (5)$$

the r component of the momentum equation

$$\frac{d}{dz}T_r = F_r, \quad (6)$$

where

$$T_r(z) \equiv \int_{r_s}^{r_1} 2\pi r m_i n v_z v_r dr \quad F_r(z) \equiv - \int_{r_s}^{r_1} 2\pi r \frac{\partial}{\partial r} (n T_e) dr, \quad (7)$$

the z component of the momentum equation

$$\frac{dT_z}{dz} = F_z, \quad (8)$$

where

$$T_z(z) \equiv \int_{r_s}^{r_1} 2\pi r (n m_i v_z^2 + n T_e) dr \quad F_z(z) \equiv - \int_{r_s}^{r_1} 2\pi r \left(m_e n v_z \frac{\omega_c^2}{\nu} \right) dr, \quad (9)$$

and the energy equation

$$\Gamma_\varepsilon(z) \equiv \int_{r_0}^{r_1} 2\pi r \left\{ \left[\frac{m_i}{2} (v_r^2 + v_z^2) + \frac{5}{2} T_e \right] n v_z + q_z \right\} dr = \Gamma_{\varepsilon 0} = \text{const.} \quad (10)$$

Here $r_s = (r_0 + r_1)/2$ for the slab and $r_s = r_0$ for the solid cylinder. The assumption of a radial magnetic field only holds for the thin annular beam. The cylindrical beam will be assumed unmagnetized.

We now transform the equations for fluid variables that depend on z and r to equations for the radially averaged quantities that depend on z only, where the averaged quantity $\langle f \rangle(z)$ is defined as

$$\langle f \rangle(z) \equiv \frac{\int_{r_s}^{r_1} 2\pi r n(z, r) f(z, r) dr}{\int_{r_s}^{r_1} 2\pi r n(z, r) dr}. \quad (11)$$

The temperature T_e is approximated as constant across the plume $T_e(z, r) \cong T_e(z)$ due to the plasma high heat conductivity along magnetic field lines. So are $\omega_c(z, r) \cong \omega_c(z)$ and $\nu(z, r) \cong \nu(z)$. Moreover, we also approximate the axial velocity v_z as constant across the plume $v_z(z, r) \cong v_z(z)$ since v_z is approximately constant at the thruster exit plane. We therefore write

$$\Gamma_0 \equiv v_z(z) \int_{r_0}^{r_1} 2\pi r n dr. \quad (12)$$

With this last relation we can express the integrals above as

$$T_r(z) \equiv m_i \Gamma_0 \langle v_r \rangle, \quad F_r(z) \equiv -T_e(z) \frac{\Gamma_0}{v_z(z)} \left\langle \frac{\partial \ln n}{\partial r} \right\rangle, \quad (13)$$

$$T_z(z) \equiv \frac{\Gamma_0}{v_z} (m_i v_z^2 + T_e), \quad F_z(z) \equiv -\Gamma_0 m_e \frac{\omega_c^2}{\nu}. \quad (14)$$

We express the averaged quantities in the following form

$$\left\langle \frac{\partial \ln n}{\partial r} \right\rangle = -\frac{\alpha}{a}, \quad (15)$$

where $a \equiv r_1 - r_s$. The energy equation becomes

$$\Gamma_{\varepsilon 0} = \Gamma_0 \left[\frac{m_i}{2} (\langle v_r^2 \rangle + v_z^2) + \frac{5}{2} T_e \right] + \frac{\Gamma_0}{v_z} \left\langle \frac{q_z}{n} \right\rangle.$$

For completeness we also present the quasi one-dimensional equation for the entropy

$$T_e \frac{d}{dz} \langle s \rangle = -\frac{d}{dz} \left(\frac{1}{v_z} \left\langle \frac{q_z}{n} \right\rangle \right) + m_e v_z \frac{\omega_c^2}{\nu}. \quad (16)$$

We now use an explicit expression for q_z

$$q_z = -\kappa \frac{dT_e}{dz}, \quad (17)$$

in which the coefficient for heat conductivity is κ and approximate $\langle 1/n \rangle = 1/n$ where $n = n(z)$ is the radially averaged plasma density at z . The governing equations for $\langle v_r \rangle$, v_z , and T_e become

$$m_i \frac{d}{dz} \langle v_r \rangle = \alpha \frac{T_e(z)}{v_z(z) a(z)}, \quad (18)$$

$$\frac{d}{dz} \left(m_i v_z + \frac{T_e}{v_z} \right) = -m_e \frac{\omega_c^2}{\nu}, \quad (19)$$

and

$$\frac{dT_e}{dz} = \frac{nv_z}{\kappa} \left[\frac{m_i}{2} (\alpha_2 \langle v_r \rangle^2 + v_z^2) + \frac{5}{2} T_e - \frac{\Gamma_{\varepsilon 0}}{\Gamma_0} \right]. \quad (20)$$

Again, we express the averaged quantity as

$$\langle v_r^2 \rangle = \alpha_2 \langle v_r \rangle^2. \quad (21)$$

We need an additional equation for the the beam thickness a , the ‘‘averaged streamline’’ equation, of the form

$$\frac{da}{dz} = \alpha_1 \frac{\langle v_r \rangle}{v_z}, \quad (22)$$

where α_1 is the assumed constant ratio between the transverse velocity at the plume boundary and the average transverse velocity.

To proceed we write an explicit expression for κ

$$\kappa = 3.16 \frac{n T_e}{m_e \nu} \left(\frac{1}{\omega_c^2 / \nu^2 + 1} \right). \quad (23)$$

From the last equation it follows that in the region of finite magnetic field in which $\omega_c \gg \nu$ the resulting heat coefficient is very small. As the magnetic field vanishes κ becomes larger.

We now write the equations (22), (18), (19), and (20) in a dimensionless form:

$$\frac{da}{d\xi} = \alpha_1 \frac{u}{v}, \quad (24)$$

$$\frac{du}{d\xi} = \alpha \frac{c^2}{va}, \quad (25)$$

$$\frac{d}{d\xi} \left(v + \frac{c^2}{v} \right) = -f_B, \quad (26)$$

and

$$\frac{dc^2}{d\xi} = \frac{1}{\kappa_n} (\alpha_2 u^2 + v^2 + 5c^2 - \Gamma_{\varepsilon n}), \quad (27)$$

for the dimensionless unknowns u , v , and c^2 with the dimensionless independent variable ξ :

$$u \equiv \frac{\langle v_r \rangle}{v_0} \quad v \equiv \frac{v_z}{v_0} \quad c^2 \equiv \frac{T_e}{m_i v_0^2} \quad \xi \equiv \frac{z}{a_0}. \quad (28)$$

In these equations f_B is the normalized magnetic force, κ_n the normalized heat conductivity, and $\Gamma_{\varepsilon n}$ the ratio of the total energy flux to the directed kinetic ion flux,

$$f_B = \frac{m_e a_0 \nu_d}{m_i v_0}, \quad \nu_d \equiv \frac{\omega_c^2}{\nu}, \quad \kappa_n = 2 \times 3.16 \times \frac{S}{\Gamma_0 a_0} \frac{n T_e}{\nu m_e} \left(\frac{1}{\omega_c^2 / \nu^2 + 1} \right), \quad \Gamma_{\varepsilon n} = \frac{2\Gamma_{\varepsilon 0}}{\dot{m} v_0^2}. \quad (29)$$

Here ν and ω_c are the electron collision and cyclotron frequencies and $\dot{m} \equiv m_i \Gamma_0$ is the mass flow rate, $v_0 = \sqrt{2e\phi_A/m_i}$, with ϕ_A , the applied voltage, and $a_0 = a(0)$. Although there is no self similar solution for

the two-dimensional equations, we assume here that the averaging parameters α , α_1 , and α_2 remain constant along the plume axis. Also $S = S(z)$ is the effective cross section of the beam,

$$S = \pi (4r_s)^{2-d} a^d, \quad (30)$$

and $d = 1$ for a slab geometry, $d = 2$ for a cylindrical geometry. We note that if ν is proportional to n the dimensionless κ_n varies with the beam cross section and with the temperature. We also define the normalized conducted heat

$$\Delta \equiv \frac{2\kappa}{m_i v_0^2 n v_z} \frac{dT_e}{dz} = \Gamma_{\varepsilon n} - (\alpha_2 u^2 + v^2 + 5c^2).$$

The electron collision frequency is the sum of electron-ion collision frequency ν_{e-i} and of additional ‘‘anomalous’’ collisions frequency ν_{ano} . We assume that the plasma is nearly fully ionized so that electron-neutral collisions are negligible. We therefore write

$$\nu = \nu_{e-i} \left(1 + \frac{\nu_{ano}}{\nu_{e-i}} \right), \quad \nu_{e-i} = 2.91 \times 10^{-6} \ln \Lambda \ n T_e^{-3/2}, \quad (31)$$

where $\ln \Lambda$ is the Coulomb logarithm, n is in cm^{-3} and T_e in eV. The anomalous collision frequency was taken as Bohm diffusion $\nu_{ano} = \alpha_B \omega_c$ with a somewhat smaller than the classical value of the Bohm coefficient, $\alpha_B = 1/80$ (as in Refs. [23, 24]). With this expression we write the normalized heat conductivity in the form

$$\kappa_n = \kappa_{nac} \frac{c^{2p} a^d}{(\omega_c^2 / \nu^2 + 1) (1 + \nu_{ano} / \nu_{e-i})} \quad (32)$$

Usually we take

$$\kappa_{nac} = 3.48 \times 10^{-7} \left(\frac{m_i}{m_e} \right) \frac{a_0 T_{e0}^p \pi}{\dot{m} \ln \Lambda c_0^{2p}} \left(\frac{4r_0}{a_0} \right)^{2-d} \left(\frac{\text{kg}}{\text{ms} (\text{eV})^p} \right), \quad p = \frac{5}{2} \quad (33)$$

We solve the equations by specifying boundary conditions upstream

$$v(0) = 1 \quad a(0) = 1 \quad u(0) = u_0 \quad c^2(0) = c_0^2 \quad (34)$$

and we require that

$$c^2(\infty) = 0, \quad (35)$$

which determines the value of $\Gamma_{\varepsilon n}$ and the amount of heat conducted Δ .

In the next section we present a brief analysis of the isothermal case using our set of equations. The results of that analysis are similar to previous analyses of the isothermal case that provided self-similar solutions of the flow.^{16,17}

IV. The isothermal case

In the isothermal case $c^2(z) = c_0^2$ being constant. We also assume that the magnetic field is zero so that the axial velocity is constant as well, $v(z) = 1$. We combine Eqs. (24) and (25). The resulting equation

$$\frac{d^2 a}{d\xi^2} = \frac{\beta^2}{2a}; \quad \beta^2 \equiv 2\alpha\alpha_1 c_0^2, \quad (36)$$

is integrated to

$$a'^2 = a'(0)^2 + \beta^2 \ln \frac{a}{a_0}; \quad a' \equiv \frac{da}{d\xi}, \quad a'(0) = \alpha_1 u_0 \quad (37)$$

and further to

$$\text{erf} \left[i \sqrt{\frac{a'(0)^2}{\beta^2} + \ln \frac{a}{a_0}} \right] - \text{erf} \left[i \frac{a'(0)}{\beta} \right] = \frac{i\beta}{\sqrt{\pi}} \xi \exp \left[\frac{a'(0)^2}{\beta^2} \right]. \quad (38)$$

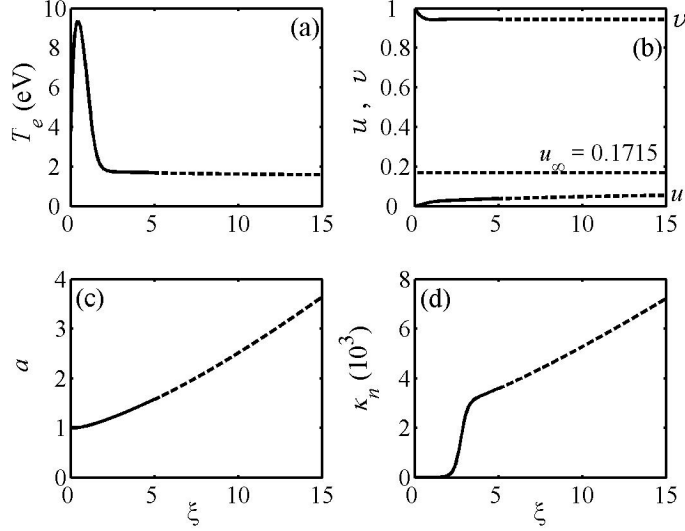


Figure 1. Characteristic slab plume profiles for the parameters mentioned in the text: (a) T_e which increases in the magnetized region, (b) the radial and axial velocities, denoted is the asymptotic radial velocity, (c) the width of the beam, and (d) the heat conductivity, much smaller in the magnetized region.

The two last relations are combined for the following relation between a' and ξ :

$$\operatorname{erf}\left(\frac{ia'}{\beta}\right) - \operatorname{erf}\left(\frac{ia'(0)}{\beta}\right) = \frac{i\beta}{\sqrt{\pi}}\xi \exp\left[\frac{a'(0)^2}{\beta^2}\right]. \quad (39)$$

This last relation provides us with the value of ξ for which a' becomes of order unity. Since β is usually much smaller than unity, for $a'/\beta \gg 1$ we approximate $\operatorname{erf}(ia'/\beta) \approx i\beta/(a'\sqrt{\pi}) \exp(a'^2/\beta^2)$ so that:

$$\xi \cong \frac{1}{a'} \exp\left[\frac{a'^2 - a'(0)^2}{\beta^2}\right] + \frac{i\sqrt{\pi}}{\beta} \operatorname{erf}\left(\frac{ia'(0)}{\beta}\right) \exp\left[-\frac{a'(0)^2}{\beta^2}\right]. \quad (40)$$

The first term on the RHS shows a strong dependence on the electron temperature. If the temperature is higher by a factor of 2 the location where the plume reaches a certain value of a' is shortened by a factor $\exp(a'^2/\beta^2)$.

Since the plume expansion is so sensitive to the value of the electron temperature, it is important to examine the case that the temperature may vary. The processes that affect the temperature evolution are transfer of energy between convected thermal energy and directed energy, heat conduction and plasma heating by the electric field. In the next section we present a numerical solution without the assumption of an isothermal electrons.

V. Numerical solution of the equations in a slab geometry

Equations (24), (25), (26), and (27) were solved for various values of the input parameters, using the method described in the Appendix. Note that while in the isothermal case the structure of the equations is the same for both geometries, when heat conductivity is taken into account, the solution depends on the geometry. We start with the slab geometry which is a good approximation as long as $a \ll r_0$ for the thin annular plasma beam exiting the thruster. Equation (33) holds with $d = 1$.

The cathode is located at $z = 0$ and the plume propagates in the region $z > 0$. The profile of the magnetic field intensity was taken as

$$B = B_{\text{peak}} \exp\left[-\frac{(z - z_m)^2}{L_m^2}\right], \quad (41)$$

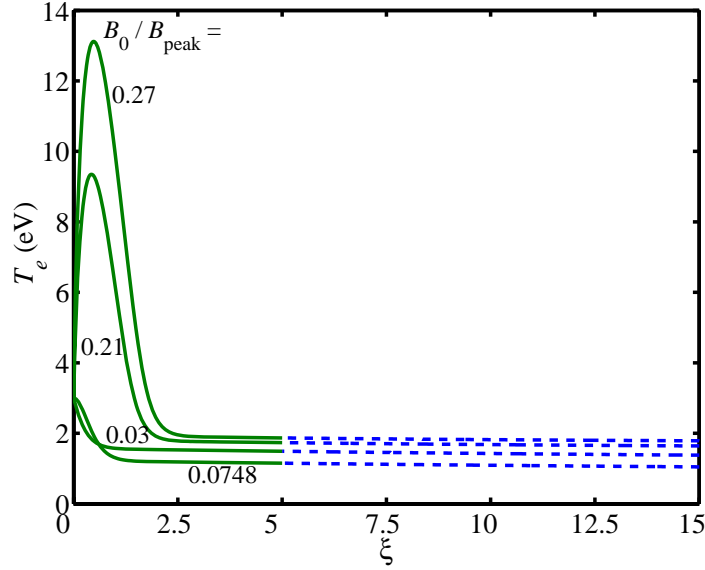


Figure 2. The temperature profile for different values of z_m in Eq. (1), denoted is the value of B_0/B_{peak} . The parameters, except for z_m are as in Fig. 1. The curve for which $B_0/B_{\text{peak}} = 0.21$ is as in Fig. 1.

with $z_m < 0$ a location inside the thruster channel and L_m being the characteristic width. Figure 1 presents the results of the calculation for a typical case $B_{\text{peak}} = 200$ G, $z_m = -30$ mm and $L_m = 20$ mm. The thruster dimensions are channel half width $a_0 = 7.5$ mm and a median radius of $r_s = 42.5$ mm. The propellant is assumed to be Xenon. At the cathode the temperature is taken as $T_e = 3$ eV, the transverse velocity as $u_0 = 0$, and $\phi_A = 300$ V. The particle flux Γ_0 was calculated for $\dot{m} = 4.76$ mg/s. The values of the three averaging parameters α , α_1 , and α_2 were taken as $3/2$, 4 , and $16/5$ respectively.

The axial profiles are presented in the near field only even though the calculation domain spans temperatures approaching zero. The solid and dashed lines show the results as found by the two different numerical schemes described in the Appendix. An important result is the temperature behavior within the magnetic field region (Fig. 1(a)). The temperature increases sharply as the magnetically impeded electrons are forced to cross the magnetic field at the same velocity as do the ions. The increase in temperature is due to the work of the ambipolar electric field, hence, the ion kinetic energy (and velocity in the z direction) decreases (Fig. 1 (b)). Curiously, until now there is only little experimental evidence for such a temperature increase.^{1,15} As the magnetic field intensity drops, κ is increased, allowing heat to flow downstream (Fig. 1 (d)). The temperature gradient in that region is inversely proportional to the fast-varying coefficient heat conductivity as the total heat flux varies slower (the total energy flux is constant). At a certain plane along the plume propagation the temperature gradient becomes smaller as some point along the plume the drop in temperature levels to much smaller gradients, this is the result of conducting heat with a much higher heat coefficient value. As the magnetic field vanishes the values of the plasma parameters match the values of the zero magnetic field calculations (dashed line). Since only the near field is presented ($z/a_0 \leq 15$), the asymptotic approach of T_e to 0 and of u to $u_\infty = u(z = \infty)$ is not apparent in Fig. 1. As is seen in Fig. 1(c) the magnetic field has two opposing effects on the electron temperature and further on the plume divergence. On one hand, the magnetic field inhibits heat flux and therefore the temperature drop is enhanced in magnetized region, resulting in a reduced plume divergence. On the other hand, the magnetic field induces an ambipolar electric field that heats the electrons, resulting in an increased plume divergence. Due to the competition between the two processes that govern the evolution of the temperature, the reduction of heat conductivity and the introduction of the ambipolar electric field, the dependence of the plume divergence on the magnetic field intensity turns out to be nonmonotonic. An optimal intensity of the magnetic field exists, at which the electron temperature of the plume exiting the magnetized region is lowest and the final plume divergence minimal. The dependencies of the electron temperature and the plume divergence on the intensity of the magnetic field are exhibited in Figs. 2 and 3. Figure 2 shows the profiles of the electron temperature for various different values of z_m , reflecting how deep into the magnetic field is the cathode

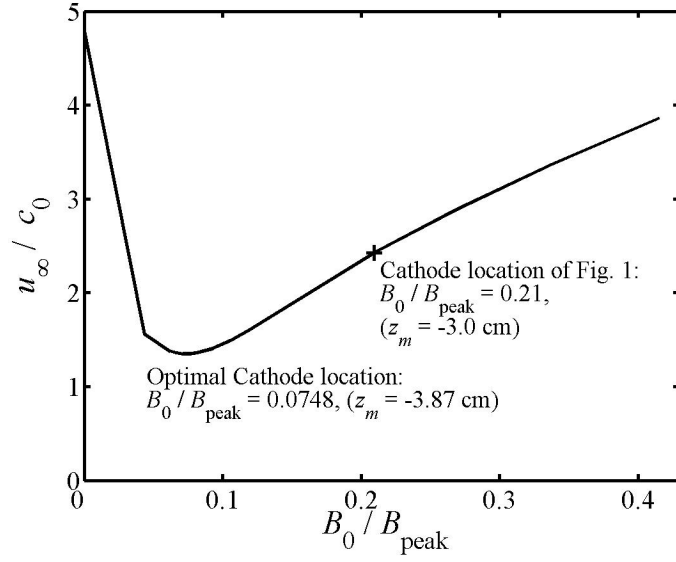


Figure 3. The asymptotic radial velocity as a function of the location of the cathode with respect to the magnetic field.

located. For the assumed identical B_{peak} , L_m and $T_e(0)$ there is an optimal value of z_m , or, equivalently, magnetic field intensity at the cathode. The asymptotic radial velocity of the plasma beam is shown in Fig. 3 as a function of the intensity of the magnetic field at the cathode. In the figures the dependence on z_m is shown by denoting $B_0/B_{\text{peak}} = \exp(-z_m^2/L_m^2)$. The existence of an optimal configuration is apparent there too.

In the next section we examine further the effect of the heat conductivity on the evolution of the plume beyond the magnetized area.

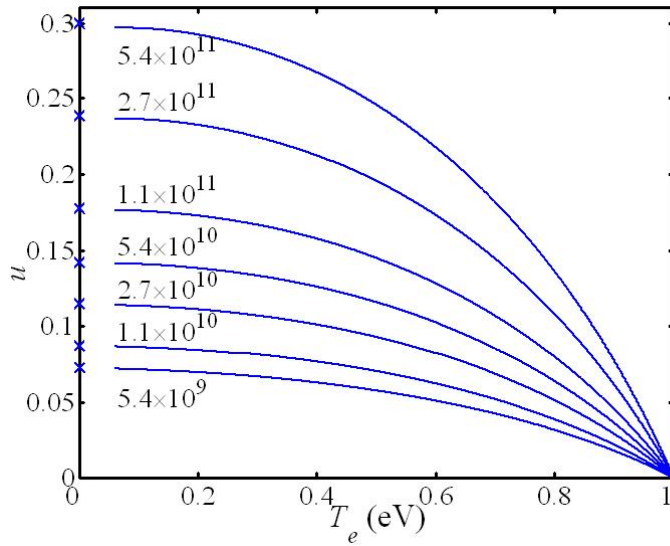


Figure 4. Unmagnetized slab beam: the radial velocity as a function of the electron temperature for different values of κ_{nac} .

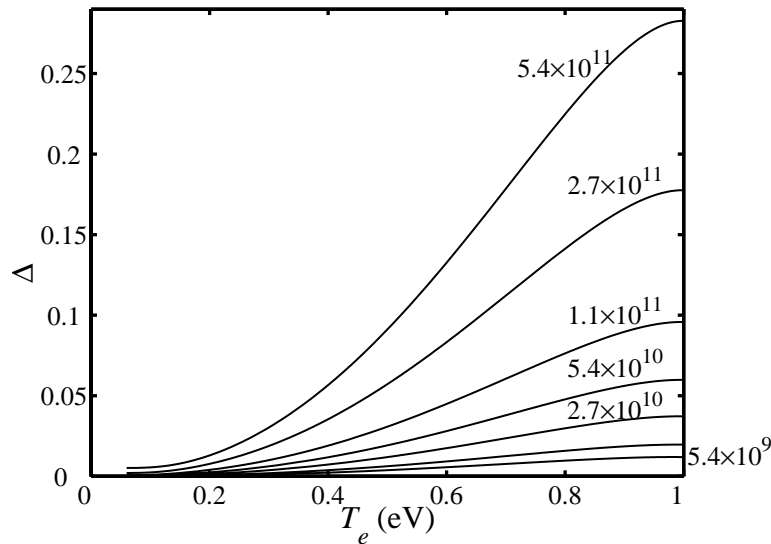


Figure 5. Unmagnetized slab beam: the conducted heat as a function of the electron temperature for various values of κ_{nac} .

VI. The effect of heat conductivity in a slab beam

Here we analyze the effect of heat conductivity on the plume evolution in the unmagnetized region. Because the magnetic-field force is zero, $f_B = 0$ in Eq. (26), the plasma momentum in the axial direction is constant,

$$v + \frac{c^2}{v} = 1 + c_0^2, \quad v_\infty = 1 + c_0^2 \quad (42)$$

because of Eq. (35). We address first the slab geometry, $d = 1$ in Eqs. (32) and Eq. (33), but we keep p unspecified,

$$\kappa_n = \kappa_{nac} c^{2p} a. \quad (43)$$

In the slab geometry the equations are reduced to one differential equation:

$$\frac{du}{dc^2} = \frac{\alpha \kappa_{nac} c^{2(1+p)}}{v (\alpha_2 u^2 + v^2 + 5c^2 - \Gamma_{\varepsilon n})}. \quad (44)$$

in which v is specified by Eq. (42) and $\Gamma_{\varepsilon n}$ is determined by the requirement that

$$\Delta(\infty) = \Gamma_{\varepsilon n} - v_\infty^2 - \alpha_2 u_\infty^2 = 0, \quad \text{when } d = 1.$$

The equation relates u and c^2 and is decoupled from the equations for the dependence on ξ . The last requirement determines the value of the eigenvalue $\Gamma_{\varepsilon n}$. It is important to note that in the slab geometry the conducted heat at infinity is zero. All the heat at the cathode, $\Delta(0) = \Gamma_{\varepsilon n} - 1 - 5c_0^2$, is converted into convected thermal energy and then into directed kinetic energy. In the slab geometry therefore the directed kinetic energy and the plume expansion are potentially large if the heat conductivity is large.

Figure 4 shows u versus T_e , while Figure 5 shows the conducted heat versus T_e , both for various values of κ_{nac} . It is seen in the figures that the heat conducted ends up in the kinetic energy associated with the radial velocity of the ions. In both figures $\phi_A = 300$ V and $p = 5/2$. The applied voltage, the ion (xenon) mass, and the initial temperature determine the value of c_0^2 , while the value of κ_{nac} is arbitrarily specified in order to examine the effect of the heat conductivity. The radial velocity is larger when κ_{nac} is larger.

We can actually derive analytical expressions for the asymptotic limit of large values of κ_{nac} .¹⁹ At that limit we approximate

$$v \cong 1 \quad \alpha_2 u^2 + v^2 + 5c^2 - \Gamma_{\varepsilon n} \cong \alpha_2 u^2 + 1 - \Gamma_{\varepsilon n}, \quad \alpha_2 u_\infty^2 + 1 - \Gamma_{\varepsilon n} = 0. \quad (45)$$

In this approximation the convected electron thermal energy is much smaller than the conducted heat. Equation (44) is then simplified to

$$\frac{du}{dc^2} = \frac{\alpha\kappa_{nac}c^{2(1+p)}}{\alpha_2(u^2 - u_\infty^2)}. \quad (46)$$

This simplified equation is integrated to

$$\left(\frac{u^3 - u_0^2}{3}\right) - u_\infty^2(u - u_0) = \frac{\alpha\kappa_{nac}}{\alpha_2} \left[\frac{c^{2(2+p)} - c_0^{2(2+p)}}{2+p}\right], \quad (47)$$

where we allowed an initial finite radial velocity $u(z=0) = u_0$. The expression for u_∞ when $u_0 = 0$ is ¹⁹

$$u_\infty = \left[\frac{3\alpha\kappa_{nac}c_0^{2(2+p)}}{2\alpha_2(2+p)}\right]^{1/3}, \quad p = \frac{5}{2} \Rightarrow u_\infty = \left(\frac{\alpha\kappa_{nac}}{3\alpha_2}\right)^{1/3} c_0^3 \quad (48)$$

Thus, the solution in the slab geometry is characterized by all the conducted heat being transformed into thermal energy and eventually perpendicular kinetic energy. The perpendicular velocity is unbounded in that geometry and increases with the initial velocity and with the size of the coefficient of heat conduction. Figure 6 shows the dependence of u_∞ on κ_{nac} for two values of initial electron temperatures. The agreement with the analytical expressions [Eq. (48) for $p = 5/2$] is excellent.

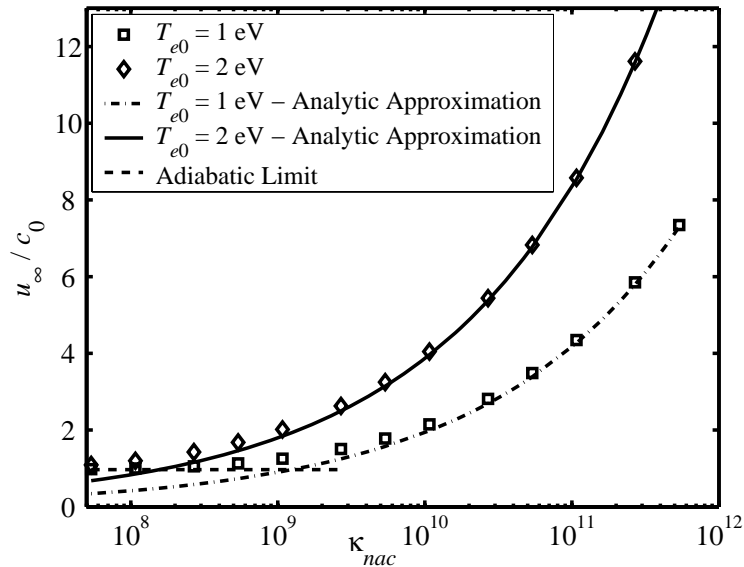


Figure 6. Unmagnetized slab beam: the asymptotic radial velocity as a function of κ_{nac} for two electron temperatures. A comparison of the analytical and numerical results. Shown is also the adiabatic case.

The growth of the radial velocity of the plasma beam as predicted by the analysis of this section is too small to explain the plume divergence observed in the near field of the thruster. For the measured electron temperatures the plane at which the plume crosses the axis of symmetry of the thruster should be further away that it actually is. We thus conclude that the main cause of the plume divergence near the exit of the plasma thruster is not the plasma pressure, but probably the magnetic field curvature.

We turn to examine the plume divergence beyond the cross-over plane. We approximate the plasma beam there as cylindrical.

VII. The effect of heat conductivity in a cylindrical beam

The governing equations in the case of a cylindrical beam are Eqs. (24), (25), (26), and Eq. (27), which, for $d = 2$ and with no magnetic field, takes the form

$$\frac{dc^2}{d\xi} = \frac{1}{\kappa_{nac}c^{2p}a^2} (\alpha_2u^2 + v^2 + 5c^2 - \Gamma_{\epsilon n}). \quad (49)$$

Because the area in the cylindrical beam is proportional to the square of the radius an equation relating u and c^2 decoupled from ξ cannot be derived as was done for the slab case. The Appendix describes the numerical scheme for solving the equations in the cylindrical case. These equations describe the basic, and of a general nature, phenomenon of a radial expansion of a beam (plasma or neutral gas) of a cylindrical geometry.

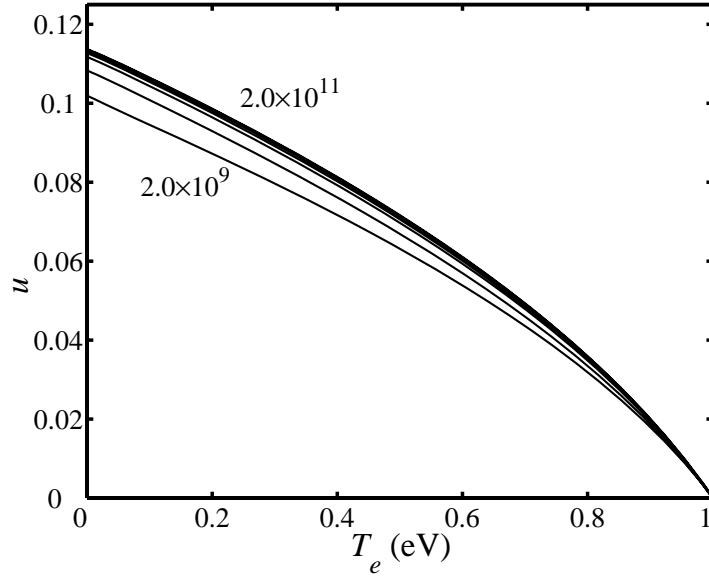


Figure 7. Unmagnetized cylindrical beam: the radial velocity as a function of the electron temperature for different values of κ_{nac} .

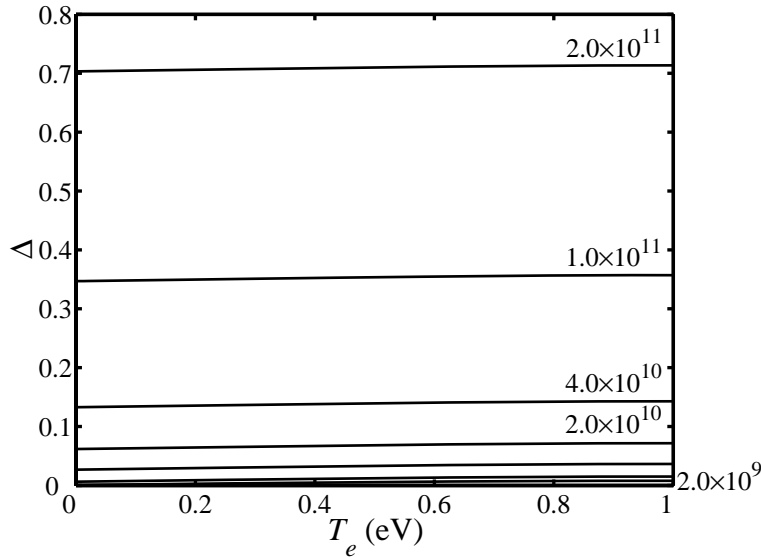


Figure 8. Unmagnetized cylindrical beam: the conducted heat as a function of the electron temperature for various values of κ_{nac} .

In the cylindrical geometry there is a weak coupling only between the conducted heat and the convected electron thermal energy. As the coefficient of heat conductivity or the initial electron temperature is increased the heat conducted is large. At the limit of large conducted heat, that heat is uniform along the beam. Let us examine this asymptotic case. The last equation is approximated as

$$\frac{dc^2}{d\xi} = -\frac{\beta_c}{\kappa_{nac}c^2\rho a^2} \quad \beta_c \equiv -(\alpha_2 u^2 + v^2 + 5c^2 - \Gamma_{\epsilon n}) \cong const > 0.$$

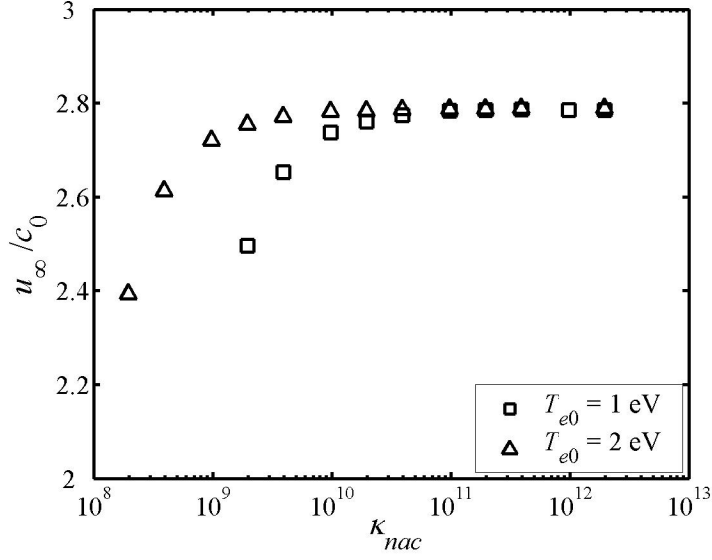


Figure 9. Unmagnetized cylindrical beam: the asymptotic radial velocity as a function of κ_{nac} for two electron temperatures. Apparent is the asymptotic limit.

Combining this equation with Eq. (24) in which we approximate $v \cong 1$, we write the following equation:

$$k \frac{d^2 k}{dt^2} = -A_c t^{1/(1+p)}, \quad k \equiv \frac{1}{a}, \quad t \equiv \left(\frac{c}{c_0} \right)^{2p+2}, \quad A_c \equiv \alpha \alpha_1 \left[\frac{c_0^{2p+3} \kappa_{nac}}{\beta_c (p+1)} \right]^2, \quad (50)$$

to be solved for

$$k(1) = 1 \quad \frac{dk}{dt}(1) = 0 \quad k(0) = 0 \quad A_c = A_c(p) \text{ eigenvalue.} \quad (51)$$

Note that A_c is independent of κ_{nac} . For example, for $p = 5/2$, A_c is found numerically to be $\simeq 1.85$. From here we obtain the conducted heat to be

$$\beta_c = \sqrt{\frac{\alpha \alpha_1}{A_c} \frac{c_0^{2p+3} \kappa_{nac}}{(p+1)}}, \quad (52)$$

which shows a strong dependence on the temperature. The velocity is found to be

$$u = \sqrt{\frac{\alpha}{\alpha_1 A_c} c_0} \frac{dk}{dt}. \quad (53)$$

The velocity (53) is proportional to the acoustic velocity and is not larger for a larger heat conductivity κ_{nac} . The temperature profile $t(k)$ is independent of the heat conductivity as well at this limit.

The lack of coupling between the conducted heat and the convected thermal energy in the cylindrical beam is a major result of this paper. A beam of a cylindrical cross section can conduct heat at a high rate while this conducted heat does not affect much the plume divergence.

For the Hall thruster the plasma beam can be approximated as a cylindrical beam beyond the cross-over of the thruster axis. At that plane the beam (regrettably...) already has a high radial velocity. It is useful to derive linear solutions for the equations in this limit of large conducted heat. In fact we derive in this linear limit of the large conducted heat cylindrical beam case analytical solutions.

We approximate the radial velocity to lowest order as constant:

$$u_0 = \sqrt{\frac{\alpha}{\alpha_1 A_c} c_0} \frac{dk}{dt} \quad (54)$$

and as before

$$k(1) = 1 \quad k(0) = 0 \quad A_c(p) \text{ eigenvalue.} \quad (55)$$

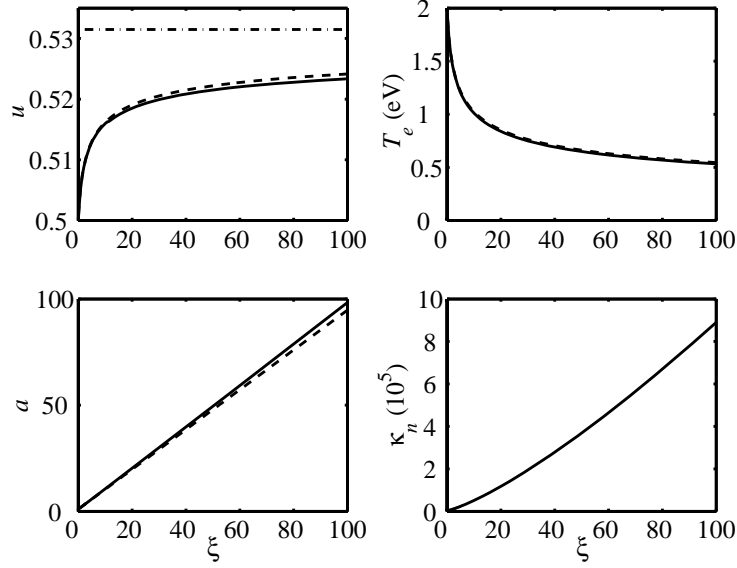


Figure 10. Cylindrical plume profiles in the linear regime - analytical (dashed?) and numerical (solid?). Also shown are the asymptotic analytical limits.

we find that

$$tu_0 = k \sqrt{\frac{\alpha}{\alpha_1 A_c}} c_0, \quad (56)$$

which, with Eq. (51) yields

$$A_c = \frac{\alpha}{\alpha_1} \left(\frac{c_0}{u_0} \right)^2, \quad \beta_c = \frac{\alpha_1 u_0 c_0^{2p+2} \kappa_{nac}}{(p+1)}. \quad (57)$$

The linear solutions are therefore

$$a_l = 1 + \alpha_1 u_0 \xi \quad c^2 = c_0^2 a_l^{-\frac{1}{p+1}} \quad u = u_0 + \frac{\alpha c_0^2 (p+1)}{\alpha_1 u_0} \left(1 - a_l^{-\frac{1}{p+1}} \right) \quad a \cong 1 + \alpha_1 u \xi. \quad (58)$$

The asymptotic value of the velocity is

$$u_1(\infty) = \frac{\alpha c_0^2 (p+1)}{\alpha_1 u_0}. \quad (59)$$

The conditions for the heat conductivity to be considered large and for the linearization to be justified are

$$\beta_c = \frac{\alpha_1 u_0 c_0^{2p+2} \kappa_{nac}}{v(p+1)} \gg 1 \quad \frac{\alpha c_0^2 (p+1)}{\alpha_1 u_0^2} \ll 1. \quad (60)$$

We now present numerical results for the cylindrical case. Figure 7 shows u as a function of T_e for various values of κ_{nac} . It is seen in the figure that as κ_{nac} grows the velocity reaches asymptotically a limit value. Similarly in Fig. 8 the normalized conducted heat is shown to be larger when κ_{nac} is larger but it does not change along the beam propagation. It is apparent in the figure that the conducted heat and the convected thermal energy are decoupled.

VIII. Summary

We presented an analysis of the plume divergence due to electron pressure of a plasma beam for both a slab and a cylindrical geometry. We have unfolded the two opposite effects of the transverse magnetic field. We have shown that the effect of the heat conductivity is very different in the two different geometries.

The results of this analysis are of a general nature and may apply to various plasma beams in laboratory and in space. In the Hall thruster the measured plume divergence seems to be much larger than the plume divergence due to the electron pressure as calculated according to the model here. We therefore suggest that the magnetic field curvature is the main cause of the plume divergence. The present analysis could also be useful to study the effects of other processes, such as charge exchange, on the plume divergence.

Appendix

As was mentioned in Section V in the case of no magnetic field in a slab geometry, the equation for v becomes an algebraic relation, and the equations for u , and c^2 are independent on ξ and are decoupled from the equation for a . This allows us to set the temperature as the independent variable and solve for the lateral velocity without dealing with infinite values of ξ and a . The equation for u (c^2) (Eq. 44) is singular at infinity ($c^2 \rightarrow 0$). In order to move away from the singularity we expand the unknowns u , v , and Δ in powers of c around $c = 0$. For the slab geometry the expansions become:

$$\begin{aligned}
 u &= u_\infty + u_2 c^2 + u_4 c^4 + u_6 c^6 + u_7 c^7 & (61) \\
 u_2 &= -\frac{3}{2\alpha_2 u_\infty} & u_4 = \frac{1}{2u_\infty} \left(\frac{1}{\alpha_2 v_\infty^2} - u_2^2 \right) & u_6 = \frac{1}{u_\infty} \left(\frac{1}{\alpha_2 v_\infty^4} - u_2 u_4 \right) & u_7 = -\frac{\alpha \kappa_{nac}}{3v_\infty} \\
 v &= v_\infty - \frac{c^2}{v_\infty} - \frac{c^4}{v_\infty^3} - \frac{2c^6}{v_\infty^5} - \frac{5c^8}{v_\infty^7} & \Delta &= -\frac{2\alpha\alpha_2\kappa_{nac}u_\infty}{3v_\infty} c^7 & u_\infty \text{ parameter}
 \end{aligned}$$

Where v_∞ is known from the algebraic relation for v and u_∞ is a parameters that is found during the solution. We use the power expansion to approximate u for a small c^2 and integrate Eq. (44) in the upstream direction. When the lateral magnetic field is present the equations are dependent on ξ through the variation of the magnetic field intensity, and the entire equation set (24) through (27) must be solved numerically. A shooting method is used to match the solutions of the two regimes; A downstream integration of the equation set is performed down to a point where the magnetic field is negligible. An upstream integration of the decoupled equation [u (c^2)] is performed from the vicinity of $c^2 = 0$ (found by the power series expansion) to the corresponding value of c^2 (at the downstream end of the zero magnetic field regime). The parameter u_∞ is adjusted by the shooting method search algorithm until the value of u is matched from both sides of the regime interface. This scheme also results in finding the corresponding value for the constant energy flux ($\Gamma_{\varepsilon n}$) as the eigenvalue of the problem. Once the value for $\Gamma_{\varepsilon n}$ is found all the other system variables (namely a and ξ), in the zero magnetic field regime, are solved as downstream as desired.

In the case of cylindrical geometry the equation for u (c^2) is not decoupled from a and we defined $k \equiv 1/a = k(c^2)$. In this case the power expansions yield:

$$k = -\alpha_1 \frac{2\kappa_{nac}u_\infty}{7\Delta_\infty v_\infty} c^7 \quad u = u_\infty - \frac{7}{2} \frac{\alpha}{\alpha_1 u_\infty} c^2 \quad u_\infty \quad \Delta_\infty \text{ parameters} \quad (62)$$

The solution was performed for the zero magnetic field regime only. The shooting method performs a search over both parameters - the heat flux (Δ_∞) and the lateral velocity (u_∞) simultaneously, yielding the initial conditions ($u(c^2 = c_0^2) = u_0$, and $k(c^2 = c_0^2) = 1$).

Acknowledgments

The authors are grateful to Prof. N. J. Fisch, Dr. Y. Raitses, Dr. J. Ashkenazy, Prof. A. Gallimore and G. Makrinich for helpful discussions. This research has been partially supported by a Grant No. 9800145 from the United States-Israel Binational Science Foundation (BSF), Jerusalem, Israel. The support of the Hellen Asher Foundation for Space Research is greatly appreciated.

References

¹ Fife, J. M., "Hybrid-PIC modeling and electrostatic probe survey of Hall thrusters," Ph.D. thesis, Massachusetts Institute of Technology, Department of Aeronautics and Astronautics, September 1998.

- ²I. Katz, G. Jongeward, V. Davis, M. Mandell, I. Mikellides, R. Dressler, I. Boyd, K. Kannenberg, J. Pollard, and D. King, "A Hall Effect Thruster Plume Model Including large-Angle Elastic scattering," AIAA Paper No. 2001-3355, *37th Joint Propulsion Conference* (American Institute of Aeronautics and Astronautics, Washington, DC, 2001).
- ³Darnon F., "The SPT-100 Plasma Plume and its Interaction with a Spacecraft, from Modeling to Ground and Flight Characterization," AIAA Paper No. 96-3196, *32nd Joint Propulsion Conference* (American Institute of Aeronautics and Astronautics, Washington, DC, 2001).
- ⁴M. Andrenucci, L. Biagioni, and A. Passaro, "PIC/DSMC Models for Hall Effect Thruster plumes: Present Status and ways Forward," AIAA Paper No. 2002-4254, *38th Joint Propulsion Conference*, Indianapolis, IN (American Institute of Aeronautics and Astronautics, Washington, DC, 2002).
- ⁵King, L. B., and Gallimore, A. D., "Ion Energy Diagnostics in the Plume of an SPT-100 from Thrust Axis to Backflow Region," *Journal of Propulsion and Power* (AIAA), Vol. 20, No. 2, March-April 2004, 193-203.
- ⁶Walker, M. L. R., Hofer, R. R., and Gallimore, A. D., "Ion Collection in Hall Thruster Plumes," *Journal of Propulsion and Power*, Volume 22, Number 1, Jan.-Feb., 2006.
- ⁷Boyd, I. D. and Dressler, R. A., "Far-field Modeling of the Plasma Plume of a Hall Thruster," *Journal of Applied Physics* Vol. 92, 2002, pp. 1764, 1774.
- ⁸Boyd, I. D. and Yim, J.T., "Modeling of the Near-Field Plume of a Hall Thruster," *Journal of Applied Physics*, Vol. 95, 2004, pp. 4575, 4584.
- ⁹Garrigues, L., Bareilles, J., Boeuf, J.-P., and Boyd, I.D., "Modeling of the Plasma Jet of a Stationary Plasma Thruster," *Journal of Applied Physics*, Vol. 91, 2002, pp. 9521, 9528.
- ¹⁰Taccogna, F, Longo, S, and Capitelli, M, "Particle-in-cell with Monte Carlo simulation of SPT-100 exhaust plumes," *Journal of Spacecraft and Rockets*, Vol. 39, 2002, pp. 409, 419.
- ¹¹Raitses, Y., Dorf, L. A., Litvak, A. A., and Fisch, N. J., "Plume Reduction in Segmented Electrode Hall Thruster," *Journal of Applied Physics*, Vol. 88, 2000, p. 1263.
- ¹²Beal, B. E., Gallimore, A. D., and Hargus, W. A., Jr., *Physics of Plasmas*, Vol. 12, 2005, Article 123503.
- ¹³Vial, V., Mazouffre, S., Prioul, M., Pagnon, D., and Bouchoule, A., *IEEE Transactions on Plasma Science* Vol. 33, 2005, p. 524.
- ¹⁴Keidar, M. and Boyd, I.D., "On the Magnetic Mirror Effect in Hall Thrusters," *Applied Physics Letters*, Vol. 87, 2005, article 121501.
- ¹⁵Karabadzhak, G. F., Chiu Y. H., and Dressler R. A., *Journal of Applied Physics*, Vol. 99, 2006, Article 113305.
- ¹⁶Parks, D. E. and Katz, I., "A Preliminary Model of Ion Beam Neutralization", AIAA 79-2049, *14th International Electric Propulsion Conference*, Princeton, NJ, 1979.
- ¹⁷Ashkenazy, J. and Fruchtman, A., "Plasma plume far field analysis," IEPC 01-260, *27th International Electric Propulsion Conference*, Pasadena, CA, USA, 2001.
- ¹⁸Cohen-Zur, A., Fruchtman, A., and Gany, A., "Analysis of the Hall Thruster Plume Divergence in the Near and Far Fields," IEPC 03-063, *28th International Electric Propulsion Conference*, Toulouse, France, 2003.
- ¹⁹Fruchtman, A. and Cohen-Zur, A., "Plume Divergence in the Hall Thruster," *Proceedings of 40th Joint Propulsion Conference and Exhibit*, 11-14, July 2004. Fort Lauderdale, FL, American institute of Aeronautics and Astronautics, Reston, VA, 2004 , AIAA Paper No. 2004-3957.
- ²⁰Fruchtman, A. and Cohen-Zur, A., "Plasma Lens and Plume Divergence in the Hall Thruster," *Applied Physics Letters*, Vol. 89, 2006, Article 111501.
- ²¹Linnell, J. A., and Gallimore, A. D., "Internal Plasma Potential Measurements of a Hall Thruster Using Plasma Lens Focusing," *Physics of Plasma*, Vol. 13, 2006, Article 103504.
- ²²Raitses, Y., Smirnov, A., and Fisch, N. J., "Enhanced performance of cylindrical Hall thrusters," *Applied Physics Letters*, Vol. 90, 2007, Article 221502.
- ²³Ahedo, E., Martinez-Cerezo, P., and Martinez-Sanchez, M., *Phys. Plasmas*, Vol. 8, 2001, p. 3058.
- ²⁴Cohen-Zur, A., Fruchtman, A., Ashkenazy, J., and Gany, A., "Analysis of the Steady-State Axial Flow in the Hall Thruster," *Physics of Plasmas*, Vol. 9, 2002, pp. 4363, 4374.